

Molecular Dynamics Study of a Nanotube-Binding Amphiphilic Helical Peptide at Different Water/Hydrophobic Interfaces

Chi-cheng Chiu, Gregg R. Dieckmann, and Steven O. Nielsen*

Department of Chemistry and Alan G. MacDiarmid NanoTech Institute, The University of Texas at Dallas, 800 West Campbell Road, Richardson, Texas 75080

Received: June 16, 2008; Revised Manuscript Received: October 22, 2008

Many potential applications of single-walled carbon nanotubes (SWNTs) require that they be isolated from one another. This may be accomplished through covalent or noncovalent SWNT functionalization. The noncovalent approach preserves the intrinsic electrical, optical, and mechanical properties of SWNTs and can be achieved by dispersing SWNTs in aqueous solution using surfactants, polymers, or biomacromolecules like DNA or polypeptides. The designed amphiphilic helical peptide nano-1, which contains hydrophobic valine and aromatic phenylalanine residues for interaction with SWNTs and glutamic acid and lysine residues for water solubility, has been shown to debundle and disperse SWNTs, although the details of the peptide–SWNT interactions await elucidation. Here we use fully atomistic molecular dynamics simulations to investigate the nano-1 peptide at three different water/hydrophobic interfaces: water/oil, water/graphite, and water/SWNT. The amphiphilic nature of the peptide is characterized by its secondary structure, peptide–water hydrogen bonding, and peptide–hydrophobic surface van der Waals energy. We show that nano-1 has reduced amphiphilic character at the water/oil interface because the peptide helix penetrates into the hydrophobic phase. The peptide α -helix cannot match its hydrophobic face to the rigid planar graphite surface without partially unfolding. In contrast, nano-1 can curve on the SWNT surface in an α -helical conformation to simultaneously maximize its hydrophobic contacts with the SWNT and its hydrogen bonds with water. The molecular insight into the peptide conformation at the various hydrophobic surfaces provides guidelines for future peptide design.

I. Introduction

Surfactants act to lower the energetic cost of hydrophilic/hydrophobic interfaces, allowing for water-insoluble materials to be dispersed in the aqueous phase. Modern biomedical materials often incorporate hydrophobic inorganic materials which interface with biological systems.^{1–4} Various surfactants are used to modify these hydrophobic surfaces to impart dispersibility and biocompatibility. For instance, quantum dots (QDs), which contain hydrophobic materials at their cores (e.g., CdSe or Au), are coated with amphiphilic molecules to improve their colloidal stability.^{5–7} These functionalized QDs can be further conjugated with peptides or DNA for biological applications such as biomarkers or biosensors. Biocompatible molecules containing poly(ethylene glycol) (PEG) have been shown to assemble into monolayers on the surface of inorganic material such as gold.^{3,4} These self-assembled monolayers can then be used to immobilize biomolecules like proteins or DNA for further bioapplications. When introducing such interfaces in vivo, it is important to study the physical and chemical impact on both the materials and the cellular system. For example, physical adsorption of proteins on the material surface could change the surface properties or induce protein denaturation and loss of function.³

Recently, single-walled carbon nanotubes (SWNTs), namely cylinders made from sheets of sp^2 -hybridized carbon atoms, have drawn significant attention for their potential uses in material, electronic, and biological applications such as biosensors, drug delivery carriers, and artificial muscles.^{8–11} However, SWNTs are

extremely hydrophobic, leading to uncontrolled aggregation in aqueous solution and making it difficult to assemble SWNTs into useful structures. Numerous studies have reported using different types of amphiphilic molecules to disperse SWNTs in aqueous solution and stabilize the water/SWNT interface.^{12,13,8,14–19} Commonly used surfactant molecules such as sodium dodecyl sulfate (SDS) and Triton-X have been shown to noncovalently modify SWNT surfaces and increase SWNT water dispersibility.^{12,13,8,14} Macromolecules like polymers,^{15,20,21} DNA,^{17,22} and polypeptides^{23,24} have also been used to control aqueous SWNT dispersibility through noncovalent adsorption on the SWNT surface.

To overcome the hydrophobicity of SWNTs and control SWNT assembly for potential biological applications, Dieckmann et al. utilized a designed 29-residue peptide named nano-1 as the surfactant to disperse SWNTs in aqueous solution. Nano-1 is designed based on Coil- V_aL_d ²⁵ and contains four heptad repeats [denoted by $(a, b, c, d, e, f, g)_4$], with valine (Val) and phenylalanine (Phe) residues located at the a and d positions, respectively.²⁶ In an α -helical conformation of nano-1, the Phe and Val residues form the hydrophobic face of the peptide helix, while the remaining residues form the hydrophilic face. The resulting α -helix is thus amphiphilic and can act as a surfactant to disperse SWNTs in aqueous solution.²⁶ Circular dichroism (CD) studies suggested that nano-1 can adapt such α -helical conformations while dispersing SWNTs in aqueous solution, and Raman spectroscopic results indicated that the dispersed SWNTs are debundled by nano-1.^{26,27} Atomic force microscopy (AFM) studies further indicated that nano-1-dispersed SWNTs have a diameter range consistent with individual SWNTs.²⁸

* Corresponding author. E-mail: steven.nielsen@utdallas.edu.

Transmission electron microscopy (TEM) experiments showed that nano-1 helices interact with the SWNT sidewall and form crossing angles ranging from 10° to 20° vs the SWNT long axis.²⁷ Also, it has been demonstrated that by forming interhelical cross-links between glutamic acid (Glu) and lysine (Lys) side chains, nano-1-dispersed SWNTs can assemble into long fibers $\sim 25 \mu\text{m}$ in diameter and several millimeters in length.²⁹ These experiments show that the nano-1 peptide can disperse SWNTs effectively and can also aid in SWNT macromolecular assembly.

A detailed picture of how the peptide interacts with the SWNT surface in aqueous solution is important to fully understand how nano-1 functions in dispersing SWNTs as well as to facilitate the design of more effective dispersal agents. The reported AFM and TEM data provide information on the nano-1–SWNT complex,^{27–29} yet the imaging was performed on dried samples which may not accurately represent the actual peptide–SWNT complex in aqueous solution. Furthermore, previous modeling of nano-1–SWNT complexes surrounded by a thin shell of water yielded energy-minimized structures.²⁶ The rationale for using molecular dynamics (MD) simulations is to explore the system conformational space that is thermally accessible at room temperature. Analysis of the resulting structures can be quantitatively compared against experimental data or used to make predictions which can be tested experimentally. In the current study, we use fully atomistic MD simulations to study nano-1 at three different water/hydrophobic interfaces: water/benzene, water/graphite, and water/SWNT. The peptide α -helical conformation and the number of hydrogen bonds formed between the peptide and water are used to evaluate the peptide stability at each interface. The interaction between the peptide and each hydrophobic surface is also analyzed to characterize the contributions from the hydrophobic residues Phe and Val.

Coil- V_aL_d forms a three-stranded coiled coil, with the three peptides supercoiled around each other.²⁵ Nano-1 has also been shown to self-associate to form three-helix bundles in solution.³⁰ The present study suggests that the supercoiling ability of the peptide helix is an important factor for nano-1 interactions with SWNT sidewalls, resulting in a stable peptide–SWNT complex. In contrast, nano-1 has a partially unfolded α -helical structure at the water/graphite interface and a reduced number of hydrogen bonds with water at the water/benzene interface. Comparing the three systems, α -helical nano-1 was found to be both energetically and conformationally stable at the curved water/SWNT interface.

II. Methods

The starting peptide coordinates for the MD simulations were generated using Insight II (Accelrys Inc., San Diego, CA) with the amino acid sequence Ac-E(VEAFEKK)-(VAAFESK)(VQAFEKK)(VEAFEHG)-CONH₂, where Ac indicates N-terminal acetylation, CONH₂ indicates C-terminal amidation, and the amino acids are represented by their single-letter abbreviations. The initial peptide conformation was set to be perfectly α -helical with backbone dihedral angles of $\phi = -65^\circ$ and $\psi = -40^\circ$. The TIP3P model was used for water molecules in all simulations.³¹ MD simulations were then performed using the program NAMD version 2.6b³² and the CHARMM31 force field.^{33–37}

All simulations were carried out in the isothermal–isobaric (NPT) ensemble with periodic boundary conditions applied in three dimensions. The pressure was controlled at 1 atm by the Nosé–Hoover Langevin piston method, and the temperature was retained at 300 K using Langevin dynamics.^{38,39} A 2 fs time

step was used to integrate the equations of motion. Electrostatic interactions were calculated using particle mesh Ewald sums. Bonds between hydrogen atoms and heavy atoms were constrained at their equilibrium lengths using the SHAKE/RATTLE algorithm.^{40,41} System coordinates were saved every 10 ps during each simulation for data analysis.

Three different water/hydrophobic systems were used in this study: (I) water/benzene, (II) water/graphite, and (III) water/SWNT. The graphite and SWNT carbon atoms were modeled using the aromatic sp^2 carbon parameters in the CHARMM31 force field. System I: the water/benzene system contained 13 054 water molecules and 1650 benzene molecules in a $100.0 \times 70.0 \times 90.0 \text{ \AA}$ box, and the helical peptide was initially placed at the planar water/benzene interface. The system was simulated for 30 ns. System II: 10 graphene layers were used in system II with an intersheet spacing of 3.4 \AA . Each layer contained 3200 carbon atoms with average x – y dimensions of $98.2 \times 85.1 \text{ \AA}$. The initial position of the peptide helix was set 8.0 \AA above the top graphene layer. The system was solvated with 10 065 water molecules, and the resulting unit cell had dimensions of $98.2 \times 85.1 \times 72.0 \text{ \AA}$. A 30 ns MD study was conducted on system II. System III: for the water/nanotube system, a (6,6) carbon nanotube with 80 cell replications was used with a length of 195.8 \AA and a diameter of 8.1 \AA , which falls in the reported diameter range of HiPco SWNTs dispersed by nano-1.²⁸ According to the experimental data, nano-1 interacts primarily with the sidewall of the SWNT; in addition, the experimental SWNT length is much longer than the accessible scale of the atomistic MD simulation.^{26–28,42} Thus, to focus our study on the peptide–SWNT sidewall interactions, we used periodic boundary conditions to effectively create an infinitely long nanotube along the x -axis. For more details of the system setup, refer to the Supporting Information. In addition, the long axis of the nanotube was immobilized on the x -axis by adding a weak additional force to the nanotube carbon atoms to prevent the nanotube from bending or tilting away from the x -axis. The additional force applied on the i th atom of the nanotube is given by eq 1:

$$F_i = -k(r_i - r_{nt}) \quad (1)$$

where r_{nt} is the nanotube radius, r_i is the instantaneous distance from the i th carbon atom to the x -axis, and k is the force constant which was set to be $1.0 \text{ kcal}/(\text{mol } \text{ \AA}^2)$ in this study. The center of mass of the peptide was initially placed 8.5 \AA away from the nanotube sidewall, and the peptide helix was oriented parallel to the nanotube long axis. The system was solvated with 22 041 water molecules in a box of dimensions $198.8 \times 64.0 \times 56.4 \text{ \AA}$. A 48 ns simulation was performed for system III. To maintain the consistencies of the water/hydrophobic interfaces, the unit cells for all three systems were fixed in the x and y dimensions during the simulations and only allowed to change in the z -direction for pressure control. After 100 ps of equilibration, the simulation cells converged to average dimensions of $100.0 \times 70.0 \times 92.3 \text{ \AA}$ for system I, $98.2 \times 85.1 \times 71.6 \text{ \AA}$ for system II, and $198.8 \times 64.0 \times 53.6 \text{ \AA}$ for system III. All three systems were considered to have reached equilibrium when both the peptide α -helicity and the root-mean-square deviation of the peptide backbone with respect to its initial conformation were converged.

The α -helicity of nano-1 was analyzed for each system to characterize the peptide conformation as the MD simulations proceeded. The α -helical content of the peptide was calculated based on the Lifson–Roig model,⁴³ where residue i is marked

α -helical only if its dihedral angle pair (ϕ_i, ψ_i) and those of the two adjacent residues ((ϕ_{i-1}, ψ_{i-1}) and (ϕ_{i+1}, ψ_{i+1})) lie in the region $(-65 \pm 35^\circ, -37 \pm 30^\circ)$. For nano-1, which has 29 residues with N-terminus acetylation and C-terminus amidation, the maximum number of residues that can be marked as α -helical is 27. The α -helicity of nano-1 can then be calculated by counting the number of α -helical residues and dividing by 27, generating a value between zero and one.

From the experimental data, nano-1 displays crossing angles ranging from 10° to 20° with respect to the SWNT long axis while interacting with the SWNT aromatic sidewall.²⁷ In this study, we analyzed the time evolution and distribution of the crossing angle in system III. The axis of the peptide helix was defined based on Kahn's model,⁴⁴ where a partial axis is defined for each four-residue segment, yielding 26 partial axes for the 29-residue peptide helix. The overall peptide helical axis was then found by using a linear least-squares method to account for all partial axes, and the crossing angle was defined as the angle formed between the helical axis and the SWNT long axis. For comparison, we also analyzed the angle between the peptide helical axis and the corresponding translation vector of the (6,6) SWNT on the top graphene layer in system II,⁴⁵ where the SWNT translation vector defines the axial direction of the nanotube formed by rolling a single graphene sheet into a cylinder.

π - π stacking interactions are incorporated into the van der Waals dispersion interaction in classical force fields and are geometrical in nature.^{46,47} In systems II and III, the distances between the aromatic ring centers of the Phe residues and the graphite or SWNT surfaces were measured to characterize the orientation of Phe side chains on the hydrophobic surfaces. In system II, the distance between a Phe residue and the top graphene layer was expressed by the z -coordinate difference between the Phe ring center and the top graphene layer. In system III, this distance was calculated by subtracting the SWNT radius (4.1 Å in this study) from the "Phe ring center to SWNT long axis" distance.

The peptide-water interaction was characterized by counting the number of hydrogen bonds (H-bonds) formed between water molecules and peptide side chains during each simulation. In this study, an H-bond was defined as follows: for a hydrogen attached to a heteroatom A, an H-bond is formed with another heteroatom B only if the distance between the two heavy atoms (AB) is smaller than 4 Å and the angle formed by atoms A, H, and B (A-H-B) is larger than 150° .⁴⁸

To study the interaction between the peptide and each hydrophobic surface, we calculated the contact area of the peptide with the hydrophobic surface. The contact area was calculated using eq 2:

$$A_{\text{contact}} = \frac{1}{2}(A_{\text{peptide}} + A_{\text{hydrophobic}} - A_{\text{complex}}) \quad (2)$$

where A_{peptide} is the molecular surface area of the entire peptide, $A_{\text{hydrophobic}}$ is the corresponding quantity for the hydrophobic phase, and A_{complex} is the whole surface area of the complex comprising the protein and the hydrophobic phase.⁴⁹ The ratio of A_{contact} to A_{peptide} was calculated to describe the degree of contact. Surface areas were calculated using the program MSMS, in which a ball of probe radius 1.4 Å is rolled around the object in question to compute the accessible surface area.⁵⁰

III. Results and Discussion

A. Peptide Conformational Analysis. Nano-1 has a maximum amphiphilicity when forming an α -helix. Thus, how the

peptide adjusts its secondary structure will affect the amphiphilicity of the peptide and its stability at the water/hydrophobic interface. Figure 1 shows snapshots of the final status of the three systems studied. For system I, nano-1 remains in an α -helical conformation at the water/benzene interface. Approximately half of the peptide helix surface area is located below the benzene surface, with all of the hydrophobic residues (Phe and Val) buried inside the oil phase (Figure 1A,B). In system II, the N-terminus of the peptide remains largely helical, while the C-terminus partially unfolds at the water/graphite interface; however, all Phe and Val residues remain in contact with the graphite surface (Figure 1C,D). In system III, the peptide is primarily α -helical at the water/SWNT interface. Also, the peptide is observed to curve on the SWNT with all hydrophobic residues are in contact with the aromatic surface of the SWNT (Figure 1E,F).

In the first 15 ns of the simulations, as shown in Figure 2, the α -helicity of nano-1 goes through rapid changes in systems II and III. These changes are due to terminal fraying. Nano-1 is able to recover its α -helicity after 20 ns and has the highest α -helical content at the water/SWNT interface. This is because the peptide can match its hydrophobic face against the curved water/SWNT interface by curving around the nanotube without disturbing its helical structure. This is not possible in system II because the interface has an extended flat geometry. After 20 ns, nano-1 remains largely α -helical over the first 15 residues (the light thin line in Figure 2) yet displays an unfolding of the C-terminal half of the sequence to permit the matching of its hydrophobic face to the flat rigid graphite surface. Because of this conformational adjustment, the total peptide α -helicity drops dramatically after 20 ns of simulation and results in a disrupted helical structure with $\sim 40\%$ total α -helicity. From a separate MD simulation with a different initial orientation of the nano-1 peptide on the graphite surface, we observed a different 15-residue segment which remains largely α -helical.⁵¹ These results suggest that on a graphite surface a sequence longer than 15 residues cannot remain helical because it cannot match its hydrophobic face to that of graphite. Which 15-residue segment remains helical depends on the initial conditions of the simulation. This suggests a peptide composed of only 15 residues [namely two heptad repeats (a, b, c, d, e, f, g)₂] might maintain a helical secondary structure better than four heptad repeats (a, b, c, d, e, f, g)₄ on a flat impenetrable hydrophobic surface. System I is unique in that its hydrophobic phase is flexible and penetrable. Here nano-1 has more conformational freedom which yields a high α -helical content. The temporary loss of α -helicity at around 20 ns is caused by terminal fraying of the helix. From the Ramachandran analysis (Figure 3), the difference in the (ϕ, ψ) angle distributions of nano-1 between the first and last 3 ns of the simulation in both systems I and III fall in the α -helical region, indicating that the peptide remains α -helical in these two systems. This is in contrast to system II, where the (ϕ, ψ) distribution shifts outside the α -helical region, again revealing the disruption of the α -helical conformation at the water/graphite interface. In addition, the (ϕ, ψ) angle distribution in system II is not randomly scattered but rather located around $(-105 \pm 25^\circ, 10 \pm 20^\circ)$ which results from modifying the helical structure at the C-terminus to conform to a flat graphite surface.

Figure 4 displays the crossing angle distributions for systems II and III. In system III, nano-1 has a wide crossing angle distribution from 5° to 25° , with the most probable angle at $\sim 17^\circ$ on the SWNT surface. This angle range encompasses the reported TEM data.²⁷ In system II, the peptide has a wider

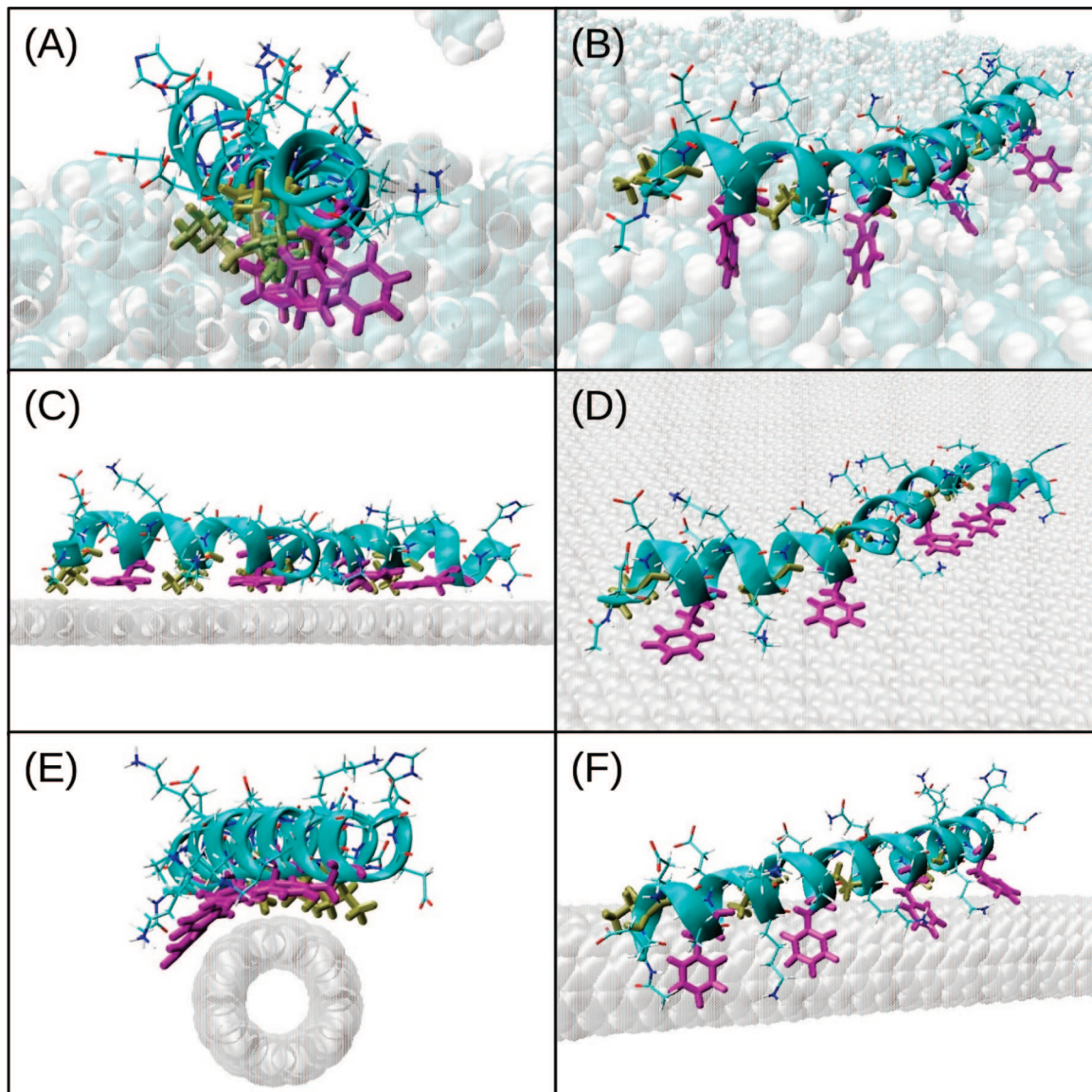


Figure 1. Representative nano-1 configurations from the MD simulations for systems I (A and B), II (C and D), and III (E and F). For each system, two different views are shown: (A), (C), and (E) display the systems approximately edge on to the water/hydrophobic interface; (B), (D), and (F) display the systems rotated slightly to give a different perspective of how the peptide interacts with the three hydrophobic surfaces. In snapshots (C) and (D), only the top graphene layer is shown. For all snapshots, water molecules have been removed for clarity. The peptide backbone is visualized using a ribbon. Nano-1 side chains are shown with a stick model, where Phe and Val residues are emphasized using thicker lines colored in purple and tan, respectively. The hydrophobic surfaces are shown using a transparent vdW model. The images were created using VMD.⁵⁴

overall crossing angle range from 40° to -25° . From the peptide α -helicity and Ramachandran analyses, the peptide has a lower α -helicity content after 20 ns. In the first 20 ns of the simulation, we find the crossing angle distribution in the range from 30° to -25° (Figure 4B), which is almost twice the angle distribution range in system II. This observation is reasonable since there is no curvature or chirality for the graphite surface, so positive and negative values of the crossing angle are equivalent. The most probable value is $\sim 12^\circ$, which is slightly different from that observed for system III; this might be due to the curvature difference between the flat and the cylindrical interfaces in systems II and III.

The geometry of the Phe side chains on the graphite and the SWNT surfaces was characterized through measuring the Phe-to-surface distance. As illustrated in Figure 5, the Phe-to-aromatic surface distance in both systems II and III has a narrow distribution, with the most probable distance at 3.5 Å. This

distance suggests that the Phe aromatic side chains align parallel with both the SWNT and graphite surfaces and is indicative of π - π stacking.^{47,52}

B. Characterization of Peptide Amphiphilic Properties. Nano-1 is amphiphilic and so can interact with the hydrophobic surface and also form H-bonds with water molecules to relieve the interfacial energy. Thus, the number of H-bonds nano-1 forms with water at different interfaces affects its stability and its surfactant nature. As shown in Figure 6, nano-1 forms more H-bonds at the water/SWNT interface than at the water/benzene interface. Furthermore, from our previous study, the number of H-bonds which are formed at the water/SWNT interface is comparable to that in pure water.⁵³ The water/SWNT interface can be viewed as a curved and rigid hydrophilic/hydrophobic interface where the peptide helix cannot penetrate into the hydrophobic phase. This allows the hydrophilic residues close to the interface to still be surrounded by water molecules.

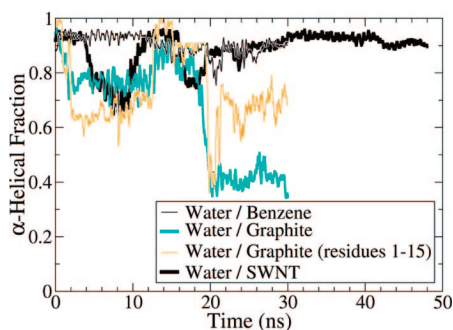


Figure 2. Nano-1 α -helicity at the water/benzene (dark thin line), water/graphite (light thick line for the entire peptide and light thin line for residues 1–15 only), and water/SWNT (dark thick line) interfaces as a function of time. The peptide retains high α -helical content in the water/benzene and the water/SWNT systems. At the water/graphite interface, the α -helicity drops dramatically after 20 ns due to a conformational adjustment of the peptide to the flat graphite surface, where the first 15 residue segment (light thin line) still retains around 70% α -helicity and the C-terminal two heptads decrease in helicity.

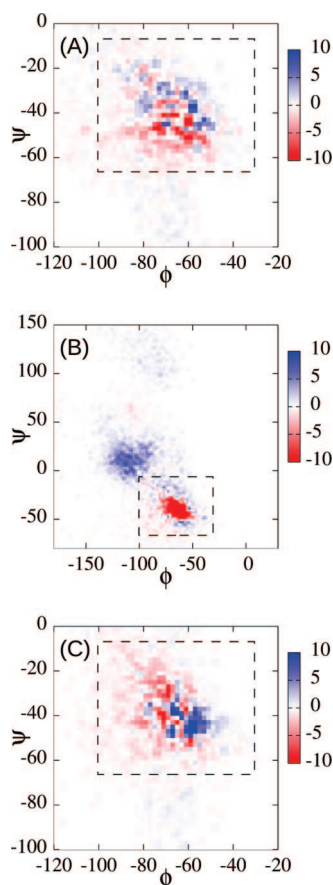


Figure 3. Difference Ramachandran plots for the changes of the (ϕ, ψ) distribution (red: decrease; blue: increase) between the first and the last 3 ns of the simulations in (A) the water/benzene, (B) the water/graphite, and (C) the water/SWNT systems. The α -helical region ($-65 \pm 35^\circ$, $-37 \pm 30^\circ$) is shown with a dashed rectangle. It is clear that the peptide remains largely α -helical at the water/benzene and water/SWNT interface. For the water/graphite system, the (ϕ, ψ) distribution shifts toward $(-105 \pm 25^\circ, 10 \pm 20^\circ)$ which is caused by partial unfolding of the C-terminus. Note the scale difference for system II (B) versus systems I (A) and III (C).

Conversely, at the water/benzene interface, the peptide can diffuse into the oil phase, limiting the H-bonding ability of the hydrophilic side chains. For the water/graphite system, before the dramatic loss of α -helicity at ~ 20 ns, the number of H-bonds

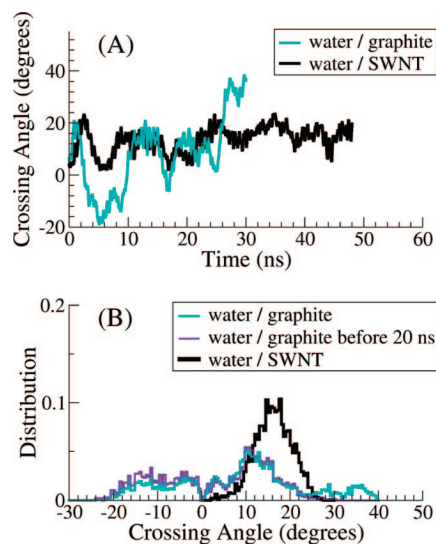


Figure 4. (A) Crossing angle formed between the peptide helical axis and either the translational vector of the (6,6) SWNT on the top graphene layer (light thick line) or the long axis of the (6,6) SWNT (dark thick line) as a function of time. (B) Crossing angle distributions of the water/graphite system counting the overall 30 ns simulation (light thick line) or only 20 ns before the loss of α -helicity (dark thin line) compared with the angle distribution of the water/SWNT system (dark thick line). Before the dramatic α -helicity loss at 20 ns, the crossing angle range for the graphite system is symmetric about zero.

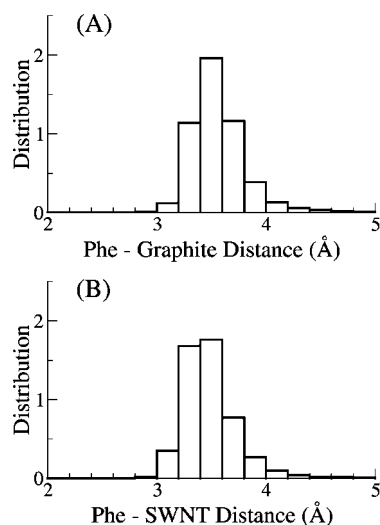


Figure 5. Distributions of the distance between the four Phe aromatic ring centers and the surface of (A) graphite or (B) SWNT. The most probable distance is ~ 3.5 Å for both systems, indicating a parallel π - π stacking conformation of the Phe side chains on both the graphite and SWNT surfaces.

is close to that of the water/SWNT system. After the α -helicity decrease, however, the number of H-bonds increases due to the disruption of the peptide secondary structure, allowing more water molecules to interact with individual residues.

Because nano-1 can diffuse into the benzene phase in system I, the peptide uses 40–45% of its overall surface area to contact the benzene molecules (Figure 7A). The large fluctuations of the peptide–benzene contact area result from peptide movement perpendicular to the interface. In the case of the flat, rigid water/graphite interface, the peptide maximizes its contact with graphite and has a contact area of 20–25% of the peptide surface area before the loss of α -helicity at 20 ns. After 20 ns, the contact area fraction increases slightly and converges to 27%. In system III, the peptide helix curves to match the cylindrical

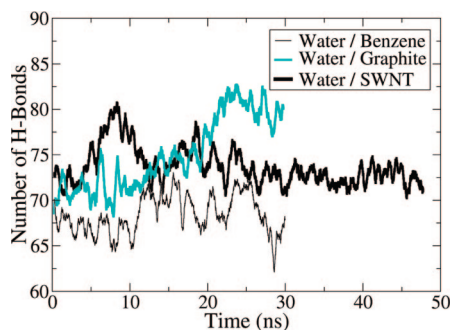


Figure 6. Number of H-bonds formed between water and peptide side chains for the water/benzene (thin line), water/graphite (light thick line), and water/SWNT (dark thick line) systems. At the water/benzene interface, nano-1 forms the fewest number of H-bonds with water. At the water/graphite interface, the number of H-bonds increases significantly after the loss of α -helicity at 20 ns.

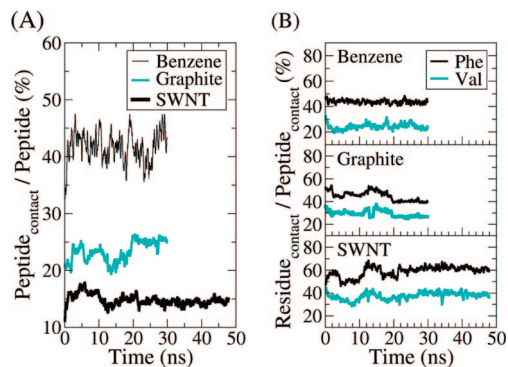


Figure 7. (A) Ratio of the contact areas between the peptide and the hydrophobic surface vs the total peptide surface area for the three systems as a function of time. Nano-1 has the largest and the smallest contact ratios at the water/benzene (thin line) and water/SWNT (dark thick line) interfaces, respectively. At the water/graphite interface (light thick line), the contact ratio changes from $\sim 20\%$ to $\sim 27\%$ after the loss of helicity at 20 ns. (B) Ratio of the Phe/Val-hydrophobic surface contact area vs the overall peptide-hydrophobic surface contact area for the three systems as a function of time. At the water/benzene interface, Phe (dark line) and Val (light line) have the smallest contributions among the three systems. At the water/SWNT interface, Phe and Val have the largest contributions among the three systems. At the water/graphite interface, the contributions of Phe and Val decrease and converge to $\sim 40\%$ and 27% , respectively, after the loss of helicity at 20 ns.

water/SWNT interface. This leads to the smallest contact area ratio among the three systems. Nonetheless, this contact area ratio has the smallest fluctuations among the three systems, suggesting a stable peptide conformation on the SWNT surface.

Next, we calculated the contribution of the hydrophobic residues (Phe and Val) to the peptide-hydrophobic surface contact area (Figure 7B). In system I, because the peptide is buried in the benzene phase, Phe and Val only contribute 40% and 20%, respectively, to the overall contact area. The remainder of the contribution comes from hydrophilic residues which decreases the surfactant-like properties of nano-1. At the water/graphite interface, Phe and Val provide $\sim 50\%$ and 30% , respectively, of the overall peptide-graphite contact area before the loss of α -helicity at 20 ns. After 20 ns, the contributions from Phe and Val decrease and converge to $\sim 40\%$ and 27% , respectively, due to an increase of the peptide-graphite contact area after the peptide adjusts its secondary structure. The convergence of the Phe and Val contributions and the overall peptide contact area after 20 ns suggests that the peptide has found a favorable conformation in contact with the graphite

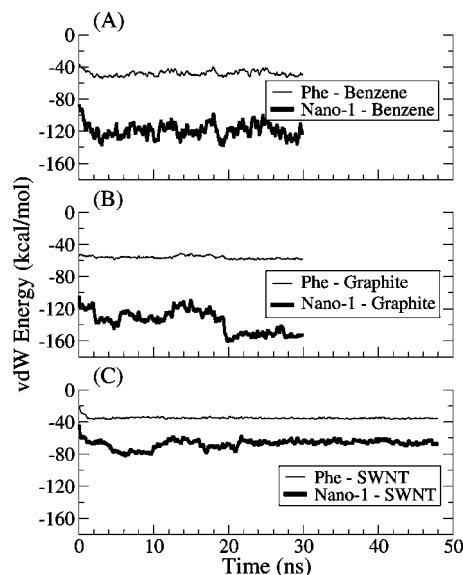


Figure 8. van der Waals interactions (vdW) between the whole peptide (thick line) or Phe residues only (thin line) and the hydrophobic surfaces. The vdW interaction energy has the largest fluctuations at the water/benzene interface (A). At the water/graphite interface (B), the vdW interaction energy changes after the loss of the helicity at 20 ns. At the water/SWNT interface (C), the vdW interaction energy is the smallest in magnitude and has the smallest fluctuations among the three systems. In all three systems, the Phe-hydrophobic surface vdW interactions have low fluctuations over time and contribute significantly to the total peptide-surface vdW energy.

surface. In the case of the water/SWNT interface, Phe and Val contribute $\sim 60\%$ and 40% , respectively, to the overall peptide-SWNT contact area which accounts for the entire peptide-SWNT contact area. This shows that the peptide uses only its hydrophobic face to contact the SWNT. The hydrophilic residues can interact with water molecules which maximizes the amphiphilic nature of the peptide.

To characterize the contribution of the aromatic residues to the enthalpy of interaction (Figure 8), we compared the absolute van der Waals (vdW) interaction energy of the whole peptide with each of the hydrophobic surfaces vs the vdW interaction energy of Phe side chains only with the hydrophobic surfaces. The rationale for using the vdW interaction energy here is because the π - π interaction between aromatic compounds is parametrized into the vdW dispersion parameters in classical force fields.⁴⁶ The magnitude of these energies in the three systems differ due to the different densities and orientations of the aromatic faces of the hydrophobic surfaces. At the water/benzene interface in system I, the peptide can penetrate into the oil phase, allowing other residues to interact with benzene molecules. Thus, the overall peptide-benzene interactions are sensitive to the depth of the peptide at the interface, leading to large variations in the vdW energy. Despite the location of the peptide, Phe residues still have a significant vdW interaction with the benzene molecules (approximately -50 kcal/mol), which is approximately 40% of the overall peptide-benzene vdW energy. In the case of the water/graphite interface (system II), the vdW energy between the peptide and the graphite is approximately -130 kcal/mol before the α -helicity decrease at 20 ns. After 20 ns, the peptide backbone of the C-terminal two heptads partially unfolds and the vdW energy changes to approximately -150 kcal/mol, corresponding to an increase of the peptide-graphite contact area. This suggests that amino acid side chains can have significant interactions with graphite which can overcome the α -helix conformational energy. The vdW

energy between Phe residues and graphite remains at approximately -60 kcal/mol and contributes 46% (before peptide unfolding at 20 ns) and 40% (after peptide unfolding) to the overall peptide-graphite vdW energy. For the peptide-SWNT system (system III), the peptide has a vdW interaction of -66 kcal/mol with the SWNT, where 55% (-36 kcal/mol) is contributed from the Phe-SWNT vdW interactions. The overall peptide-SWNT interaction is substantially smaller than the peptide-graphite or peptide-benzene interactions because the number of aromatic faces that the peptide can interact with on the SWNT surface is fewer than that on the graphite surface or in the benzene phase. On the other hand, the peptide-SWNT vdW energy has the smallest fluctuations among three systems, indicating a stable peptide-SWNT interaction. In all three systems, the Phe side chains contribute over 40% of the overall peptide-surface vdW interaction energy. Furthermore, although we see relatively large fluctuations in the overall vdW interaction energies, especially in systems I and II, the Phe interaction energy shows very small fluctuations. This suggests that conformational changes that occur in the peptide (especially in system II) are not disrupting the Phe-surface interactions. This confirms the importance of the Phe residues in the peptide for interacting with these aromatic surfaces.

IV. Conclusions

The three water/hydrophobic interfaces comprising this study have different characteristics: the water/benzene interface is flat and penetrable, the water/graphite interface is flat but impenetrable, and the water/SWNT interface is curved and rigid. These different features give rise to different amphiphilic peptide conformations. From equilibrium MD studies, we have found that nano-1 can retain its α -helical structure at the water/benzene interface where the hydrophobic phase is penetrable and the peptide has a large conformational freedom. At the water/graphite interface, the peptide must match its hydrophobic face to the flat, rigid surface, resulting in partial unfolding and a lower α -helical content. The adjustment of the peptide C-terminus secondary structure shifts the (ϕ, ψ) angle distribution toward the $(-105 \pm 25^\circ, 10 \pm 20^\circ)$ region. The conformational analysis of nano-1 on the flat graphite surface suggests that a peptide with only two heptad repeats might have a more stable helical conformation. For the water/SWNT system, the peptide matches its hydrophobic face to the cylindrical, rigid interface by curving its helical structure around the SWNT, allowing the peptide to maintain its α -helical structure on the SWNT surface. The peptide helix forms a crossing angle of 5° – 25° with the SWNT long axis, consistent with TEM measurements.²⁷

Among the three water/hydrophobic systems, the peptide forms the least number of H-bonds with water molecules at the water/benzene interface because the peptide can penetrate into the benzene phase, limiting the H-bonding ability of the hydrophilic side chains. Peptide movement normal to the interface also increases the contact area and vdW interaction between the hydrophilic residues and the benzene molecules. This decreases the importance of the Phe and Val residues and lessens the amphiphilic properties of the α -helical peptide. At the water/graphite interface, the peptide can form the largest number of H-bonds with water, but the peptide cannot preserve its α -helical structure over the entire peptide length, allowing residues other than Phe or Val to interact with graphite. The convergence of the peptide-graphite vdW energy and the Phe/Val-graphite contact area indicates that a partially unfolded helical structure is a favorable conformation for the nano-1 peptide on the graphite surface. At the water/SWNT interface,

the peptide can form as many H-bonds as in the water/graphite system before the loss of α -helicity at 20 ns. Also, the Phe and Val residues contribute 100% of the overall peptide-SWNT contact area, showing that the peptide uses only its hydrophobic face to interact with the SWNT surface. These results indicate the α -helical peptide uses its amphiphilic character optimally at the water/SWNT interface. For all three systems, the Phe-hydrophobic surface vdW energies were constant throughout the simulations. This suggests that the π - π interactions between the Phe side chains and the aromatic faces of the hydrophobic phases dominate over peptide secondary structural considerations. The overall vdW energy contributions from the Phe residues are greater than 40% in all three systems, particularly in the peptide-SWNT complex, where 66% of the overall peptide-SWNT interactions are due to Phe.

In summary, nano-1 can form a stable α -helical structure at the water/SWNT interface. The results show that nano-1 is an excellent surfactant molecule for the water/SWNT interface. The curving of the α -helical peptide allows the peptide to match its hydrophobic face with the curved SWNT surface. Further studies are needed to understand the dependence of α -helical stability on the curvature of the hydrophobic surface (i.e., as a function of the SWNT radius). We postulate that there exists a threshold curvature at which the adsorbed peptide undergoes a conformational change. In addition, by altering the pattern of hydrophobic residues in the peptide sequence, we may be able to change the hydrophobic pattern of the peptide helix and modulate its crossing angle and curvature on the SWNT surface. Reducing the sequence length to two heptad repeats (~ 15 residues) or adding a flexible linker between the second and third heptads in nano-1 are possible strategies to optimize nano-1 for interaction with a graphite surface. The implications of such altered sequences are currently being explored both experimentally and computationally.

Acknowledgment. The authors acknowledge the Donors of the American Chemical Society Petroleum Research Fund (SON) and a grant from the Human Frontier Science Program (GRD; grant RGY0070/2005-C) for partial support of this research. The authors thank Ekta Khurana for stimulating discussions and Donald W. Moore for technical assistance. The authors also acknowledge the Texas Advanced Computing Center (TACC) at The University of Texas at Austin for providing HPC resources that have contributed to the research results reported within this paper.

Supporting Information Available: Details of the water/SWNT system setup and the density profile of the water/benzene system. This material is available free of charge via the Internet at <http://pubs.acs.org>.

References and Notes

- (1) Engel, E.; Michiardi, A.; Navarro, M.; Lacroix, D.; Planell, J. A. *Trends Biotechnol.* **2008**, *26*, 39–47.
- (2) Moghimi, S. M.; Hunter, A. C.; Murray, J. C. *FASEB J.* **2005**, *19*, 311–330.
- (3) Castner, D. G.; Ratner, B. D. *Surf. Sci.* **2002**, *500*, 28–60.
- (4) Tirrell, M.; Kokkoli, E.; Biesalski, M. *Surf. Sci.* **2002**, *500*, 61–83.
- (5) Bruchez, M.; Moronne, M.; Gin, P.; Weiss, S.; Alivisatos, A. P. *Science* **1998**, *281*, 2013–2016.
- (6) Parak, W. J.; Gerion, D.; Pellegrino, T.; Zanchet, D.; Mischeel, C.; Williams, S. C.; Boudreau, R.; Le Gros, M. A.; Larabell, C. A.; Alivisatos, A. P. *Nanotechnology* **2003**, *14*, R15–R27.
- (7) Michalet, X.; Pinaud, F. F.; Bentolila, L. A.; Tsay, J. M.; Doose, S.; Li, J. J.; Sundaresan, G.; Wu, A. M.; Gambhir, S. S.; Weiss, S. *Science* **2005**, *307*, 538–544.
- (8) Lin, Y.; Taylor, S.; Li, H. P.; Fernando, K. A. S.; Qu, L. W.; Wang, W.; Gu, L. R.; Zhou, B.; Sun, Y. P. *J. Mater. Chem.* **2004**, *14*, 527–541.

- (9) Katz, E.; Willner, I. *ChemPhysChem* **2004**, *5*, 1085–1104.
- (10) Lacerda, L.; Bianco, A.; Prato, M.; Kostarelos, K. *Adv. Drug Delivery Rev.* **2006**, *58*, 1460–1470.
- (11) Baughman, R. H.; Cui, C. X.; Zakhidov, A. A.; Iqbal, Z.; Barisci, J. N.; Spinks, G. M.; Wallace, G. G.; Mazzoldi, A.; De Rossi, D.; Rinzler, A. G.; Jaschinski, O.; Roth, S.; Kertesz, M. *Science* **1999**, *284*, 1340–1344.
- (12) Vaisman, L.; Wagner, H. D.; Marom, G. *Adv. Colloid Interface Sci.* **2006**, *128*, 37–46.
- (13) O'Connell, M. J.; Bachilo, S. M.; Huffman, C. B.; Moore, V. C.; Strano, M. S.; Haroz, E. H.; Rialon, K. L.; Boul, P. J.; Noon, W. H.; Kittrell, C.; Ma, J. P.; Hauge, R. H.; Weisman, R. B.; Smalley, R. E. *Science* **2002**, *297*, 593–596.
- (14) Ke, P. C. *Phys. Chem. Chem. Phys.* **2007**, *9*, 439–447.
- (15) O'Connell, M. J.; Boul, P.; Ericson, L. M.; Huffman, C.; Wang, Y. H.; Haroz, E.; Kuper, C.; Tour, J.; Ausman, K. D.; Smalley, R. E. *Chem. Phys. Lett.* **2001**, *342*, 265–271.
- (16) Johnson, R. R.; Johnson, A. T. C.; Klein, M. L. *Nano Lett.* **2008**, *8*, 69–75.
- (17) Zheng, M.; Jagota, A.; Semke, E. D.; Diner, B. A.; Mclean, R. S.; Lustig, S. R.; Richardson, R. E.; Tassi, N. G. *Nat. Mater.* **2003**, *2*, 338–342.
- (18) Gao, H. J.; Kong, Y. *Annu. Rev. Mater. Res.* **2004**, *34*, 123–150.
- (19) Tasis, D.; Tagmatarchis, N.; Bianco, A.; Prato, M. *Chem. Rev.* **2006**, *106*, 1105–1136.
- (20) Curran, S. A.; Ajayan, P. M.; Blau, W. J.; Carroll, D. L.; Coleman, J. N.; Dalton, A. B.; Davey, A. P.; Drury, A.; McCarthy, B.; Maier, S.; Strevens, A. *Adv. Mater.* **1998**, *10*, 1091.
- (21) Tang, B. Z.; Xu, H. Y. *Macromolecules* **1999**, *32*, 2569–2576.
- (22) Zheng, M.; Jagota, A.; Strano, M. S.; Santos, A. P.; Barone, P.; Chou, S. G.; Diner, B. A.; Dresselhaus, M. S.; McLean, R. S.; Onoa, G. B.; Samsonidze, G. G.; Semke, E. D.; Usrey, M.; Walls, D. J. *Science* **2003**, *302*, 1545–1548.
- (23) Arnold, M. S.; Guler, M. O.; Hersam, M. C.; Stupp, S. I. *Langmuir* **2005**, *21*, 4705–4709.
- (24) Witus, L. S.; Rocha, J. D. R.; Yuwono, V. M.; Paramonov, S. E.; Weisman, R. B.; Hartgerink, J. D. *J. Mater. Chem.* **2007**, *17*, 1909–1915.
- (25) Ogihara, N. L.; Weiss, M. S.; Degrad, W. F.; Eisenberg, D. *Protein Sci.* **1997**, *6*, 80–88.
- (26) Dieckmann, G. R.; Dalton, A. B.; Johnson, P. A.; Razal, J.; Chen, J.; Giordano, G. M.; Munoz, E.; Musselman, I. H.; Baughman, R. H.; Draper, R. K. *J. Am. Chem. Soc.* **2003**, *125*, 1770–1777.
- (27) Dalton, A. B.; Ortiz-Acevedo, A.; Zorbas, V.; Brunner, E.; Sampson, W. M.; Collins, L.; Razal, J. M.; Yoshida, M. M.; Baughman, R. H.; Draper, R. K.; Musselman, I. H.; Jose-Yacamán, M.; Dieckmann, G. R. *Adv. Funct. Mater.* **2004**, *14*, 1147–1151.
- (28) Zorbas, V.; Ortiz-Acevedo, A.; Dalton, A. B.; Yoshida, M. M.; Dieckmann, G. R.; Draper, R. K.; Baughman, R. H.; Jose-Yacamán, M.; Musselman, I. H. *J. Am. Chem. Soc.* **2004**, *126*, 7222–7227.
- (29) Xie, H.; Ortiz-Acevedo, A.; Zorbas, V.; Baughman, R. H.; Draper, R. K.; Musselman, I. H.; Dalton, A. B.; Dieckmann, G. R. *J. Mater. Chem.* **2005**, *15*, 1734–1741.
- (30) Ortiz-Acevedo, A.; Nguyen, J. H.; Dieckmann, G. R. The University of Texas at Dallas, Richardson, TX. Unpublished work.
- (31) Jorgensen, W. L.; Chandrasekhar, J.; Madura, J. D.; Impey, R. W.; Klein, M. L. *J. Chem. Phys.* **1983**, *79*, 926–935.
- (32) Phillips, J. C.; Braun, R.; Wang, W.; Gumbart, J.; Tajkhorshid, E.; Villa, E.; Chipot, C.; Skeel, R. D.; Kale, L.; Schulten, K. *J. Comput. Chem.* **2005**, *26*, 1781–1802.
- (33) Feig, M.; MacKerell, A. D.; Brooks, C. L. *J. Phys. Chem. B* **2003**, *107*, 2831–2836.
- (34) Mackerell, A. D. *J. Comput. Chem.* **2004**, *25*, 1584–1604.
- (35) MacKerell, A. D.; Feig, M.; Brooks, C. L. *J. Am. Chem. Soc.* **2004**, *126*, 698–699.
- (36) Mackerell, A. D.; Feig, M.; Brooks, C. L. *J. Comput. Chem.* **2004**, *25*, 1400–1415.
- (37) Buck, M.; Bouguet-Bonnet, S.; Pastor, R. W.; MacKerell, A. D. *Biophys. J.* **2006**, *90*, L36–L38.
- (38) Feller, S. E.; Zhang, Y. H.; Pastor, R. W.; Brooks, B. R. *J. Chem. Phys.* **1995**, *103*, 4613–4621.
- (39) Martyna, G. J.; Tobias, D. J.; Klein, M. L. *J. Chem. Phys.* **1994**, *101*, 4177–4189.
- (40) Andersen, H. C. *J. Comput. Phys.* **1983**, *52*, 24–34.
- (41) Ryckaert, J. P.; Ciccotti, G.; Berendsen, H. J. C. *J. Comput. Phys.* **1977**, *23*, 327–341.
- (42) Zorbas, V.; Smith, A. L.; Xie, H.; Ortiz-Acevedo, A.; Dalton, A. B.; Dieckmann, G. R.; Draper, R. K.; Baughman, R. H.; Musselman, I. H. *J. Am. Chem. Soc.* **2005**, *127*, 12323–12328.
- (43) Lifson, S.; Roig, A. *J. Chem. Phys.* **1961**, *34*, 1963–1974.
- (44) Kahn, P. C. *Comput. Chem.* **1989**, *13*, 185–189.
- (45) Saito, R.; Dresselhaus, G.; Dresselhaus, M. S. *Physical Properties of Carbon Nanotubes*; Imperial College Press: London, 1998.
- (46) Macias, A. T.; MacKerell, A. D. *J. Comput. Chem.* **2005**, *26*, 1452–1463.
- (47) Hunter, C. A.; Sanders, J. K. M. *J. Am. Chem. Soc.* **1990**, *112*, 5525–5534.
- (48) Luzar, A.; Chandler, D. *Phys. Rev. Lett.* **1996**, *76*, 928–931.
- (49) Ortiz, V.; Nielsen, S. O.; Klein, M. L.; Discher, D. E. *J. Mol. Biol.* **2005**, *349*, 638–647.
- (50) Sanner, M. F.; Olson, A. J.; Spehner, J. C. *Biopolymers* **1996**, *38*, 305–320.
- (51) Birdwell, D. O.; Chiu, C.-c.; Nielsen, S. O. The University of Texas at Dallas, Richardson, TX. Unpublished work.
- (52) McGaughey, G. B.; Gagne, M.; Rappe, A. K. *J. Biol. Chem.* **1998**, *273*, 15458–15463.
- (53) Chiu, C.-C. M.S. Thesis, The University of Texas at Dallas, Richardson, TX, 2007.
- (54) Humphrey, W.; Dalke, A.; Schulten, K. *J. Mol. Graphics* **1996**, *14*, 33–38.

JP805313P